A Nanoscale Shape Memory Oxide

Jinxing Zhang[1,2*†], Xiaoxing Ke[3*†], Gaoyang Gou[4], Jan Seidel[2,5], Bin Xiang[6,9], Pu Yu[2,7], Wen-I Liang[8], Andrew M. Minor[9,10], Ying-hao Chu[8], Gustaaf Van Tendeloo[3], Xiaobing Ren[4] and Ramamoorthy Ramesh[2,10]

[1] Department of Physics, Beijing Normal University, Beijing 100875, China

[2] Department of Physics, University of California, Berkeley, 94720, USA

[3] EMAT (Electron Microscopy for Materials Science), University of Antwerp, Groenenborgerlaan 171, Antwerp, 2020, Belgium

[4] Multi-disciplinary Materials Research Center, Frontier Institute of Science & Technology, Xi' an Jiaotong University, Xi' an 710049, China

[5] School of Materials Science and Engineering, University of New South Wales, Sydney NSW 2052, Australia

[6] CAS Key Laboratory of Materials for Energy Conversion, Department of Material Science and Engineering, University of Science and Technology of China, Hefei 230026, China

[7] State Key Laboratory for Low-Dimensional Quantum Physics, Department of Physics, Tsinghua University, Beijing 100084, China

[8] Department of Materials Science and Engineering, National Chiao Tung University, HsinChu 30010, Taiwan

[9] National Center for Electron Microscopy, Lawrence Berkeley National Laboratory, Berkeley 94720, USA

[10] Department of Materials Science and Engineering, University of California, Berkeley, 94720, USA

[†] These authors contributed equally to this work

* Email: jxzhang@bnu.edu.cn or xiaoxing.ke@uantwerpen.be

Supplementary information:

Supplementary Figures:

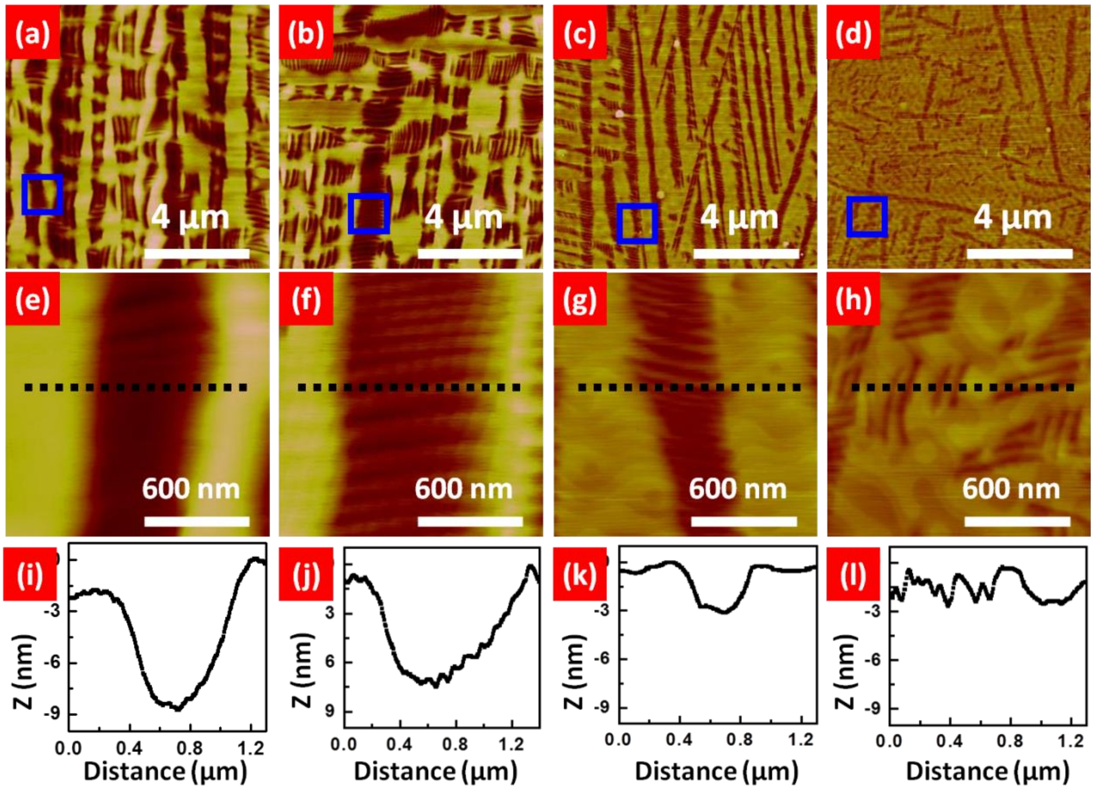

Supplementary Figure S1 | Thickness-dependent phase evolution in this strain-sensitive system. a topography (a) of a 160 nm thick film with a magnified image (e) from the highlighted blue box and a height profile along the dashed black line (i); a topography (b) of a 120 nm thick film with a magnified image (f) from the highlighted blue box and a height profile along the dashed black line (j); a topography (c) of a 80 nm thick film with a magnified image (g) from the highlighted blue box and a height profile along the dashed black line (k); a topography (d) of a 40 nm thick film with a magnified image (h) from the highlighted blue box and a height profile along the dashed black line (l). The scale bars for (a), (b), (c) and (d) are 4 μm and the ones for (e), (f), (g) and (h) are 600 nm.

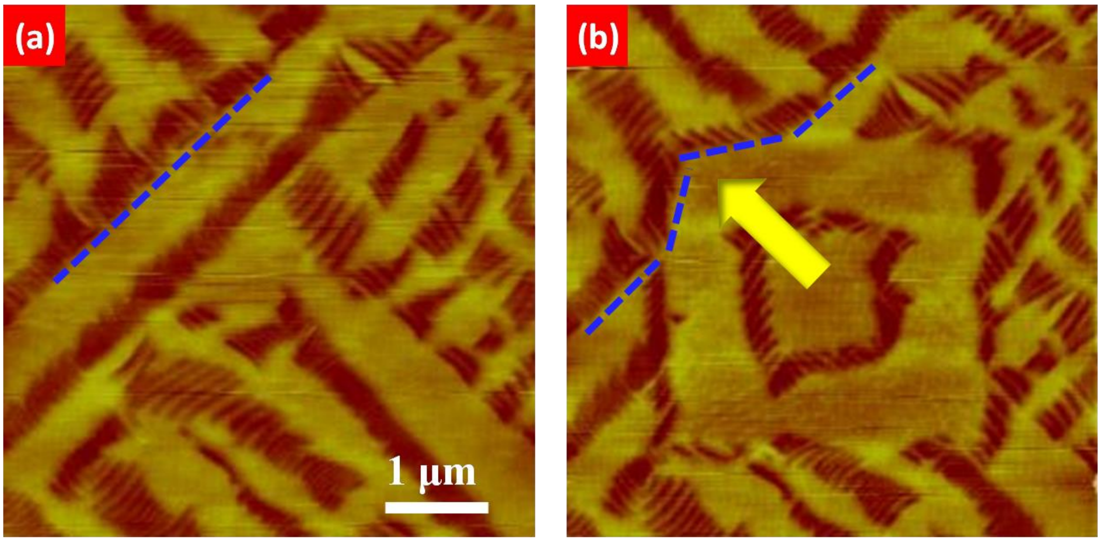

Supplementary Figure S2 | An interface (martensitic-like twin walls) movement by electric field. AFM images show a relocation of the phase boundaries in a ~120 nm thick BFO film with R/T mixture from an as-grown state (a) to a poled state (b) by a probe-scanning-electric-field of ~100 kV/cm, resembling a martensitic twin wall movement by a thermal or magnetic field in SMAs or magnetic SMAs (the dashed blue line can help guide eyes). The scale bar is 1 μm.

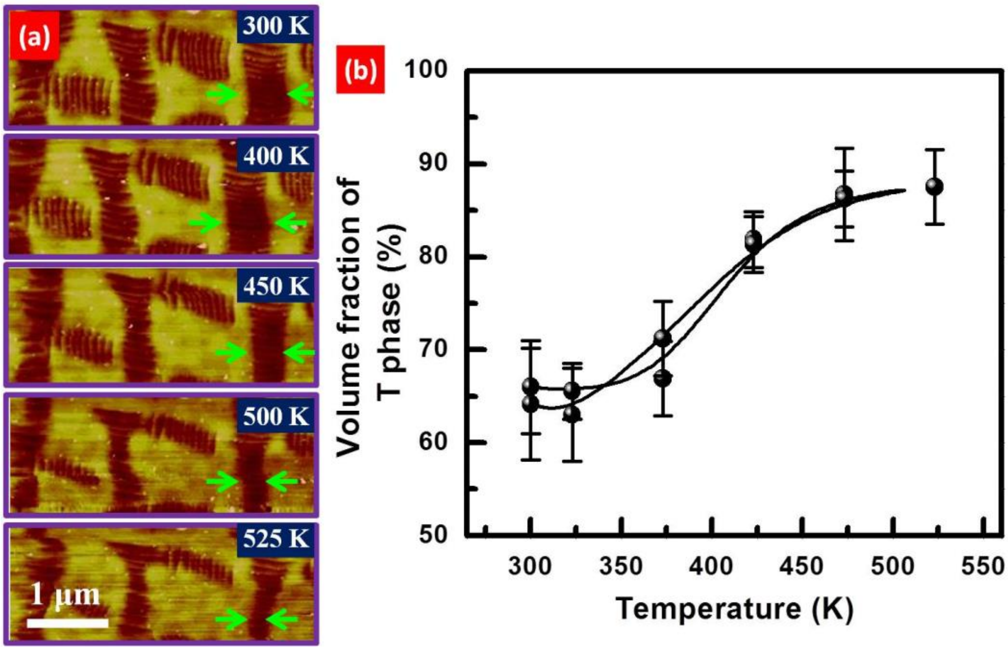

Supplementary Figure S3 | An interface (martensitic-like twin walls) movement by a thermal activation. (a) AFM images show a phase evolution as a function of temperature from 300 K to 525 K, resembling a heat induced shape recovery in the martensitic transformation of SMAs, (b) the quantitative volume fraction of the T-phase as a function of temperature, where the T-phase become stable with an elevated temperature. The scale bar is 1 μm. The error bars in (b) are from the measurement on different sample locations.

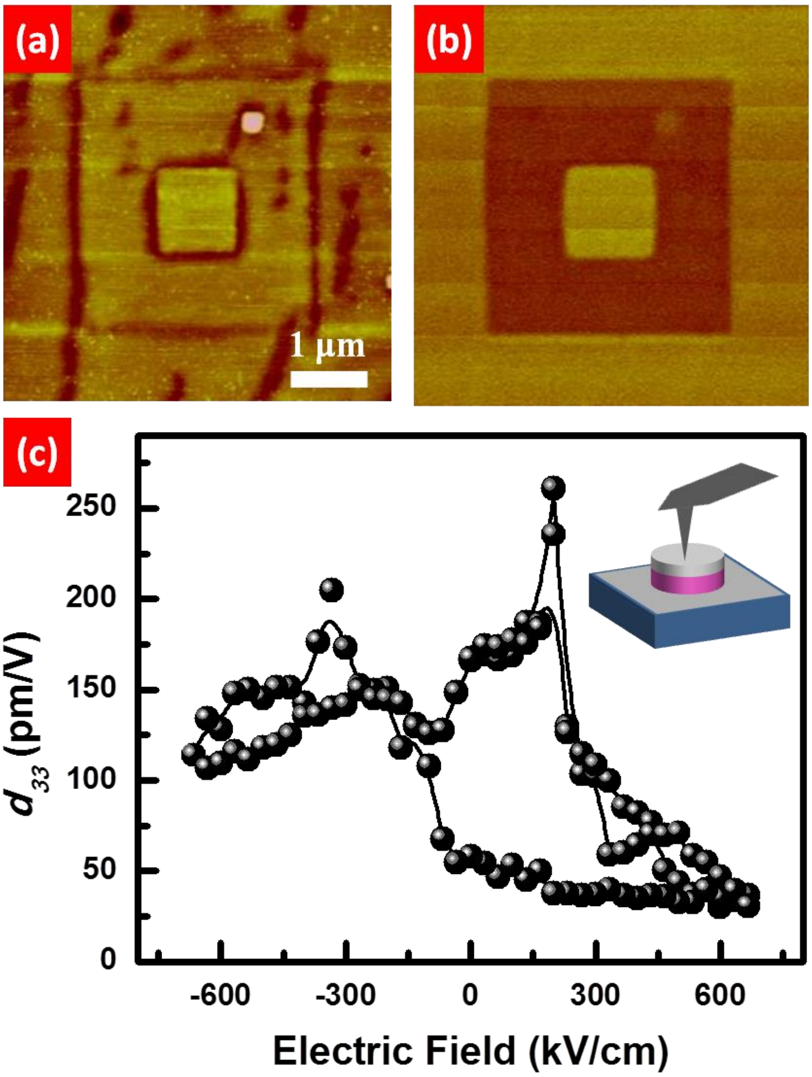

Supplementary Figure S4 | Ferroelectric switching on a clamping-removed BFO capacitor with R/T mixture. (a) topography before and after probe electric field of +667 kV/cm in 3 μm^2 and -667 kV/cm in 1 μm^2, (b) out-of-plane ferroelectric domain image before and after probe voltages of +667 kV/cm in 3 μm^2 and -667 kV/cm in 1 μm^2, showing its robust ferroelectric behavior after the removal of substrate clamping, (c) piezoresponse hysteresis loop on an clamping-removed BFO capacitor, showing the dramatic enhancement of the piezoelectric coefficient can be reversibly obtained with the application of AC and DC electric field (the inset is the measurement setup). The scale bar is 1 μm.

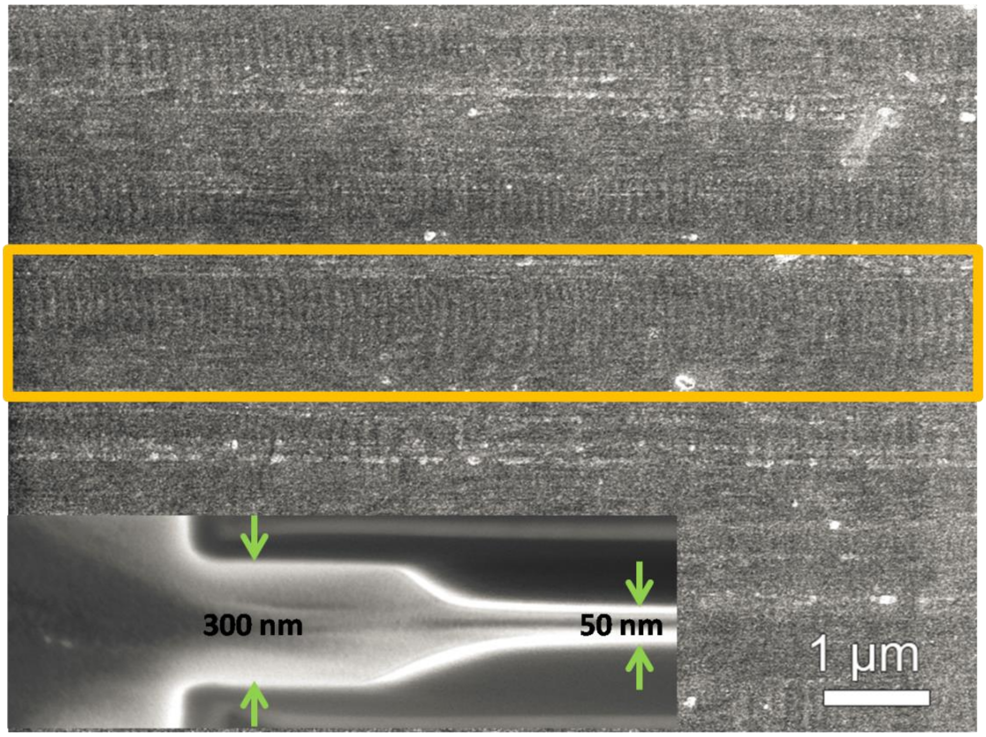

Supplementary Figure S5 | A scanning electron microscopy (SEM) image of the BFO with R/T mixture. The TEM sample with stripe-like feature has been FIB milled into a wedged-shape in the yellow box in order to study how phase evolves with the reduction of lateral size (clamping), where the inset shows the SEM top-view image of the FIB-milled sample with a gradient size from ~300 nm at left side and ~50 nm at the right side. The scale bar is 1 μm.

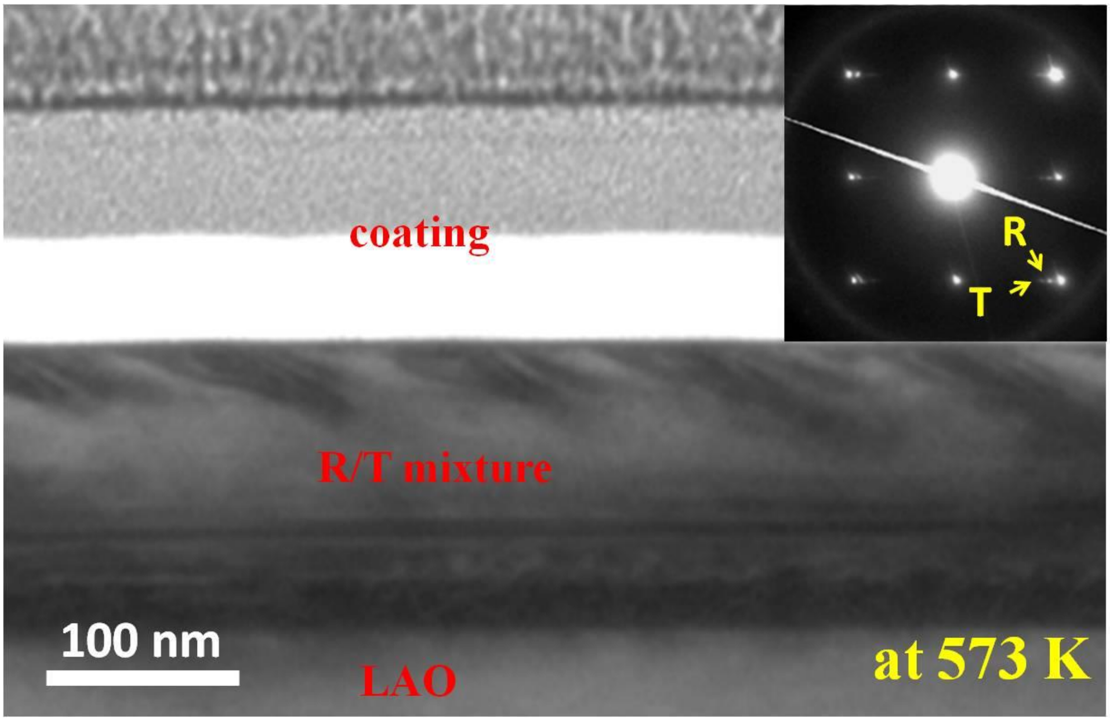

Supplementary Figure S6 | A demonstration of a partially recovery of the large SME. The image shows the low-magnification TEM image of the partially recovered BFO from a relaxed pure R-phase during the process of the heating cycles (image captured at 573 K). The typical stripe-like feature and the coexistence of diffraction patterns in the inset give the evidence of the R/T mixture during the recovery of the large SME. The scale bar is 100 nm.

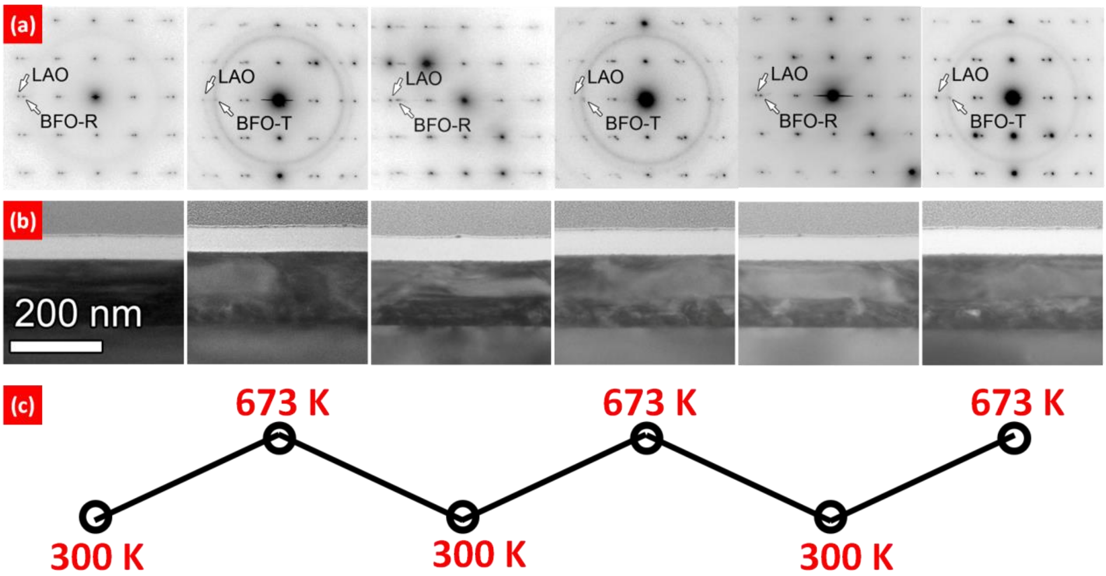

Supplementary Figure S7 | A reversible structural transformation with a large SME by temperature cycling. (a) diffraction patterns of the clamping-removed BFO during the temperature cycling, showing the reversible structural transformation between pure R-phase and pure T-phase, (b) low-magnification images of the clamping-removed BFO with an observable shape change during the temperature cycling, demonstrating a recovery strain of ~12 $\pm$ 2%, (c) the corresponding temperature cycling process. The scale bar is 200 nm.

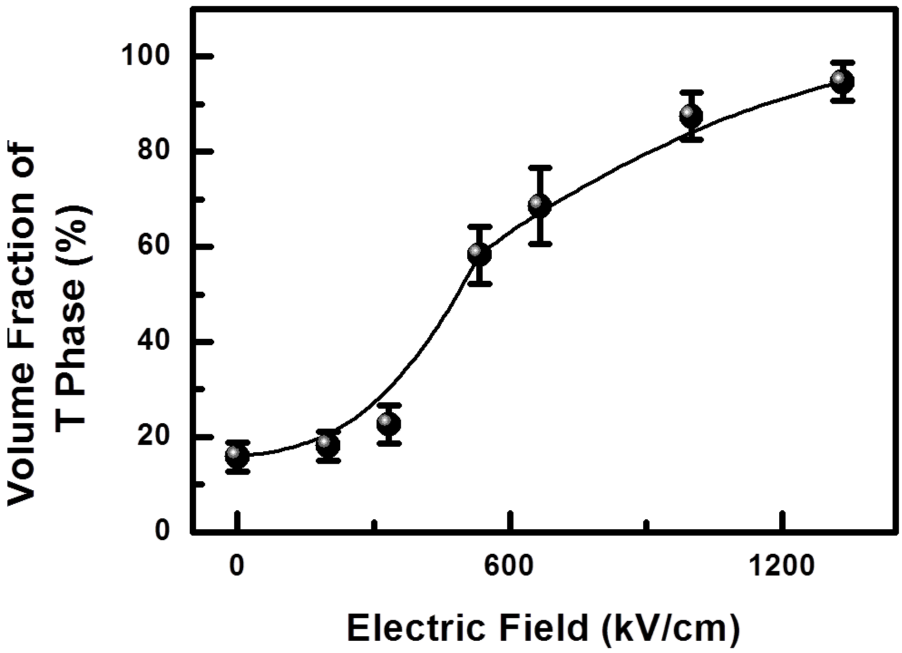

Supplementary Figure S8 | Quantitative determination of the phase evolution by electric field. Single-step control of shape memory effect with a strain of over 10% driven by a moderate electric field, associated with the transformation from rhombohedral phase to tetragonal phase. The error bar is from the measurement on different samples and locations.

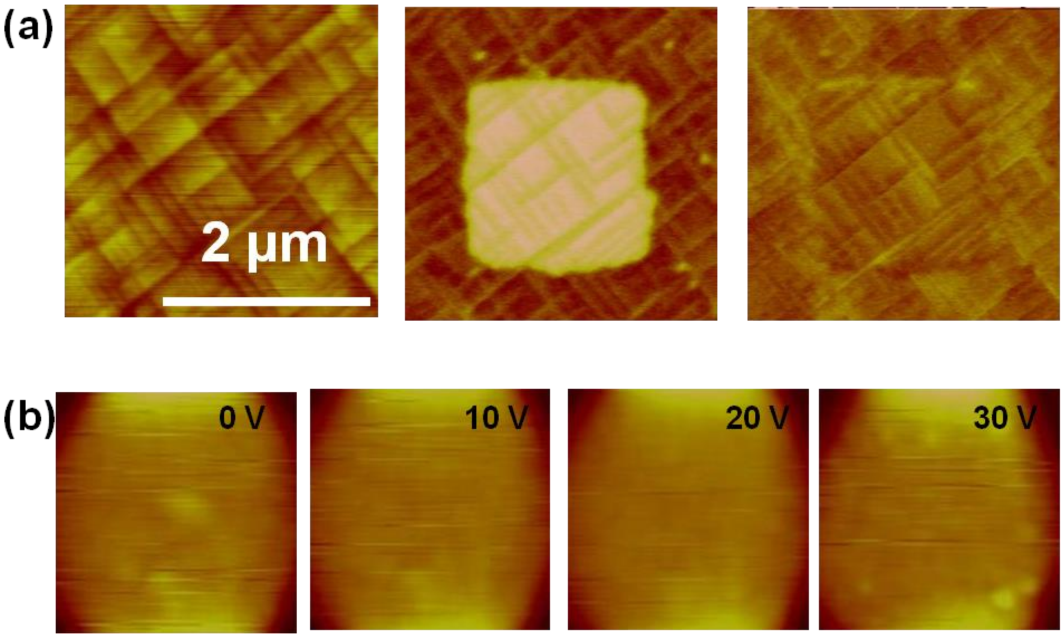

Supplementary Figure S9 | Effect of probe voltage on the unconstrained PZT structure. (a) ferroelectric switching of a constrained PZT thin film with out-of-plane and in-plane domain images, (b) probe-voltage-dependent topography on the focus-ion-beam etched PZT structure with a diameter of 1 μm and a height of 200 nm, showing no surface displacement. This experiment is used to be a comparison between unconstraint PZT and BFO, showing no large SME in this material. The scale bar is 2 μm.

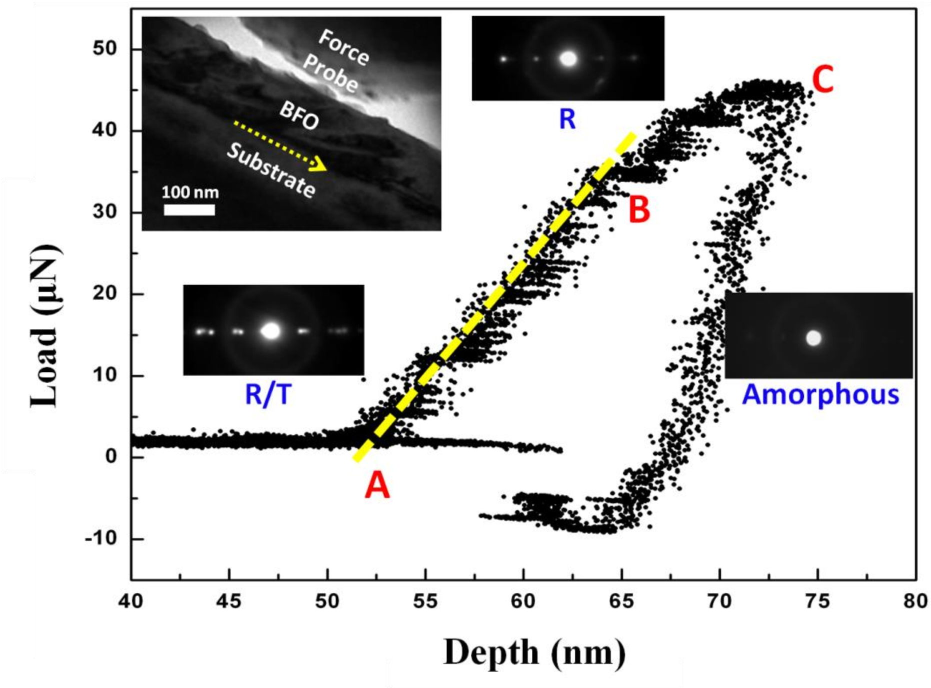

Supplementary Figure S10 | A mechanical test on the mixed-phase BFO thin film coupled with the in-situ TEM. Force/depth indentation curve obtained in a mechanical-coupled TEM as illustrated by the inserted low-magnification image (the contact geometry) on the top left. The inset TEM diffraction patterns correspond with each stage during the indentation, where stage A is R/T phase mixture, stage B is pure R phase after the application of the indented force, and C is the crushed amorphous film by the overloaded force. The plotted Young's modulus is about 70±10 GPa during the phase transformation, which is consistent with previous experimental and theoretical results. The scale bar in the inset is 100 nm.

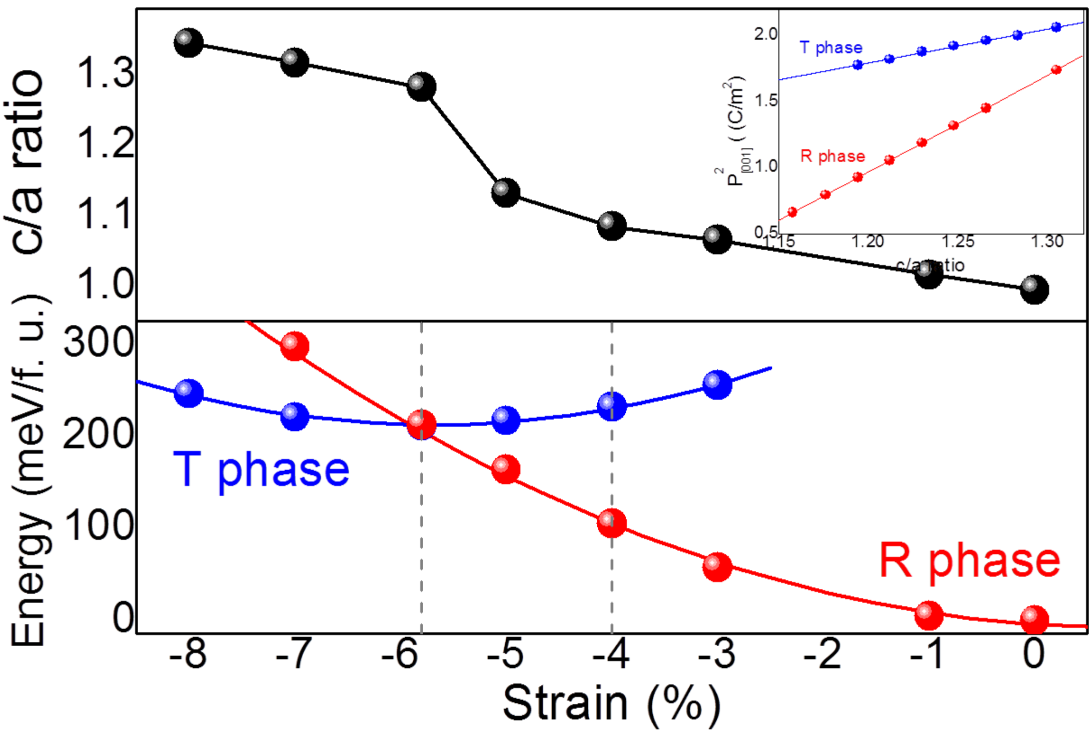

Supplementary Figure S11 | Strain-dependent properties for BFO R- (red) and T-phase (blue). Change of (upper curve) c/a ratio and (lower curve) energy of BFO phases as a function of compressive strain. A first-order phase transition between R- and T-phase can occur with epitaxial compression of about -5%. The inset gives a linear correlation between squared polarization along [001] direction and tetragonality c/a ratio, obtained from a -5.8 % strained BFO. For both R- and T-phase, their P^2 [001] are closely correlated to c/a ratio.